



# Magnetically Separable PVA-functionalized Mn-Fe Oxide Uniform Nanoparticles for Effective Removal of Cationic Dyes from Aqueous Medium

K. Akhtar, M. Gul, I. U Haq, S. A Shah, Z. U Khan

National Centre of Excellence in Physical Chemistry, University of Peshawar, Peshawar-25120, Khyber Pakhtunkhwa, Pakistan.

Received 05 Jun 2016,  
Revised 27 Feb 2017,  
Accepted 05 Mar 2017

## Keywords

- ✓ Magnetic oxide;
- ✓ Magnetic separation;
- ✓ Adsorption;
- ✓ Uniform particles;
- ✓ Coprecipitation;
- ✓ PVA functionalization

[khalida\\_akhtar@yahoo.com](mailto:khalida_akhtar@yahoo.com)  
+92919216766

## Abstract

Uniform nanoparticles of Mn-Fe oxide (MF) were prepared by the coprecipitation process under optimum experimental conditions. These particles acquired magnetism ( $MF_{mag}$ ) by the controlled heat treatment at 900 °C, which are then characterized by x-ray diffractometry (XRD), scanning electron microscopy (SEM), and energy-dispersive spectroscopy (EDS) for their structural, morphological, and elemental analysis, respectively. The same particles were functionalized with polyvinyl alcohol (PVA) and used as adsorbent for the removal of a model dye “Methylene Blue (MB)” from aqueous solutions. Effect of pH, concentration of dye & adsorbent, temperature, contact time of the adsorbent with the adsorbate dye molecules was evaluated on the adsorption process. The experimental data were analyzed by the Langmuir, Freundlich and Temkin models of adsorption, among them Langmuir model was found best fit to equilibrium data. The adsorption kinetics was found to follow the pseudo-second-order kinetic model. Thermodynamics parameters,  $\Delta G^\circ$ ,  $\Delta H^\circ$  and  $\Delta S^\circ$ , indicated that the adsorption of MB onto PVA-functionalized  $MF_{mag}$  was spontaneous, exothermic and physical in nature. It was noted that the adsorption process under study is very effective, since in most of the cases the adsorbate solutions became colourless and up to 99% dye was removed under optimum conditions. Similarly, in all cases, the adsorbents were easily separated from the adsorption mixtures by a permanent magnet. With the advantages of effective adsorption of dye and magnetic separation, the PVA-functionalized MF nanoparticles could prove to be a promising adsorbent in the wastewater treatment processes.

## 1. Introduction

Dyeing technology can be thought tantamount to man's existence in the colorful world and the use of dye products is unavoidable. However, serious problems arise when synthetic dyes are released into the environment causing pollution to man and his environment because of their slow or even no biodegradability. The contamination of water bodies by synthetic dyes has caused serious environmental issue worldwide [1]. The later cause problems in numerous manners: firstly, the presence of dyes in water, even in traces, is very much visible and unwanted because color restricts the sunlight penetration into water retarding photosynthesis and thus inhibits the growth of aquatic biota, and secondly dyes interfere with solubility of gases in water bodies [2]. These materials comprised of complicated organic aromatic compounds, which resist against light, washing and microbial invasions and therefore, cannot be decomposed easily [3]. Dyes containing effluents must be treated before discharge into municipal environments they produce toxic carcinogenic breakdown products. The basic and diazo direct dyes have been found to have the highest rates of toxicity [4, 5]. Methylene blue (MB) is one of the basic dyes, which is common practice for dyeing cotton, wood and silk. Acute exposure to MB cause several harmful effects like increased heartbeat, vomiting, nausea, cyanosis, jaundice and tissue necrosis in humans [6].

The conventional methods to remove dyes from wastewater are electrochemical treatment [7], coagulation and flocculation [8], chemical oxidation [9], liquid-liquid extraction [10] and adsorption [6,11]. Among these, adsorption technique is preferred to remove organic matter from aqueous medium in terms of simplicity, cost effectiveness, ease of handling and insensitivity to toxic substances [4]. The existing literature is rich in work conducted on the adsorption of MB onto various adsorbents like activated carbon [12,13], glass

fibers [14], rice husk [15], peanut hull [16], pineapple leaf powder [17], natural phosphate [18], fly ash [19], diatomaceous silica [20], chitosan-g-poly(acrylic acid)/ montmorillonite super adsorbent nanocomposite [3], sand [21], cyclodextrin polymer [22], PVA [23], etc. In the above-mentioned literature, the main difficulty observed is the collection of dye-loaded adsorbent to separate the dye from parent solution and recycle the adsorbent to reduce cost in practical application on large scale. The use of magnetic nanoparticles as adsorbent or adsorbent-support material is the key to address this dilemma. However, the nanoparticles must be uniform in size and shape to get batch-to-batch reproducibility in adsorption practice. Moreover, the smaller the size of particles, the larger will be the surface area of given amount and hence the lesser quantity of adsorbent will remove significant concentration of dye from water thereby reducing the cost.

In the present work, Mn-Fe oxide nanoparticles synthesized with greater uniformity were coated with polyvinyl alcohol (PVA) and applied as magnetically separable adsorbent to remove MB from aqueous medium. Figure 1 shows the chemical structures of PVA and MB. PVA was selected as coating material because of its ease of attachment to metal oxide surfaces through hydrogen bonding [24] and occurrence in deprotonated form (negatively charged) in normal pH range [23]. As such, it seems feasible for practical application on large scale as low cost material for the removal of cationic dyes from the aqueous medium.

The main objective of this research was the development of an efficient, low cost and magnetically separable adsorbent for the removal of dyes from aqueous medium. Methylene blue was taken as the model dye in this study and its removal from aqueous solutions was evaluated as a function of pH, contact time, concentration of dye and adsorbent.

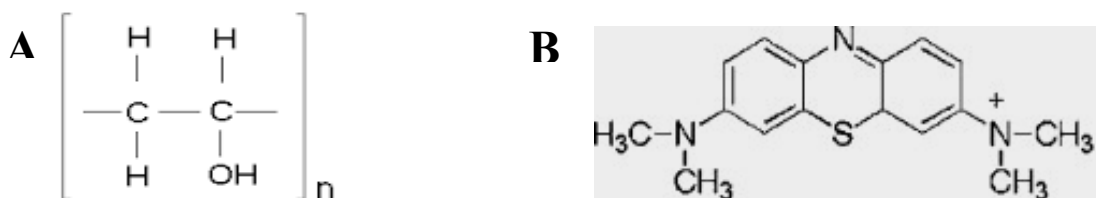


**Figure 1.** Chemical structure of Polyvinyl alcohol ((A) and methylene blue (B).

## 2. Experimental details

### 2.1. Materials

Materials used for the synthesis of Mn-Fe oxide nanoparticles were  $\text{MnSO}_4$  (Scharlau),  $\text{Fe}(\text{NO}_3)_3 \cdot 9\text{H}_2\text{O}$  (Scharlau),  $\text{NH}_4\text{OH}$  (BDH, England), PVA (BDH England) and Methylene blue dye (Merck). To adjust pH of dye solution,  $0.01 \text{ mol.L}^{-1}$  aqueous solutions of HCl and NaOH were used. All the chemicals were of analytical grade and were employed without any purification. De-ionized water was used to prepare stock and working solutions.

### 2.2 Synthesis of Mn-Fe Oxide Nanoparticles

Aqueous solutions containing  $\text{Mn}^{2+}$  and  $\text{Fe}^{3+}$  species ( $0.1 \text{ M}$  each) in the ratio  $\text{Fe}^{3+}/\text{Mn}^{2+} = 2$  were mixed and heated to  $353 \text{ K}$  in a double walled Pyrex glass vessel. During the entire precipitation process, the reaction mixture was constantly stirred using a magnetic stirrer (WiseStir MSH-20D). Sufficient amount of  $3 \text{ mol.L}^{-1}$   $\text{NH}_4\text{OH}$  was added to the heated mixture to complete precipitation of metal ions and the precipitates formed were stirred for 3 h at room temperature. After aging for overnight, the mother liquor was discarded, precipitates were washed with distilled water to  $\text{pH} = 7$  and then dried in an electric oven (BINDER FD53) at  $373 \text{ K}$  ( $\pm 2 \text{ K}$ ) for 20 h.

The precipitates obtained were calcined at  $1173 \text{ K}$  for 2 h in an electric furnace (Nabertherm, L5/11) in air atmosphere, which transformed the precipitated non-magnetic metal hydroxide precursors into the magnetic metal oxides.

### 2.3 Coating of $\text{MF}_{\text{mag}}$ nanoparticles with PVA

The aqueous PVA solution (5%) was prepared by dissolving PVA in distilled water. The  $\text{MF}_{\text{mag}}$  nanoparticles were dispersed in water by sonication for 1h. Then the aqueous solution of PVA was added to the suspension of  $\text{MF}_{\text{mag}}$  in water under stirring at room temperature. After stirring for 30 min, the mixture was filtered by  $0.2 \mu\text{m}$  micropore filter paper under vacuum and washed with propanol to ensure the removal of excess PVA. The resulting nanoparticles were dried to yield PVA-functionalized  $\text{MF}_{\text{mag}}$  nanoparticles. Before adsorption, the PVA- $\text{MF}_{\text{mag}}$  nanoparticles were activated at  $371 \text{ K}$  for 1 h to remove water of hydration and surface-attached species.

## 2.4 Characterization techniques

The morphology of the synthesized particles was studied through JEOL, JSM-5910 scanning electron microscope. Precipitation of  $Mn^{2+}$  and  $Fe^{3+}$  ions from solution was confirmed through Oxford's Energy Dispersive X-ray detector (INCA 200) coupled with SEM. The X'pert PRO, PANalytical X-ray Diffractometer with  $CuK\alpha$  ( $\lambda=1.5406 \text{ \AA}$ ) radiation at step angle  $0.02^\circ$  was used to investigate crystalline nature and phase of the calcined particles. UV/Vis spectrophotometer (Spectronic 601) was used to determine the concentration of un-adsorbed dye.

## 2.5 Point of zero charge (PZC)

The point of zero charge (PZC) of PVA-functionalized  $MF_{mag}$  particles was determined by the El-sayed method [23]. The pH was determined by research grade pH electrode. For this purpose, a series of conical flasks, each containing 0.1 g PVA- $MF_{mag}$  particles dispersed in 100 mL deionized water, were arranged and sonicated for 60 min. The  $pH_i$  (initial pH) values of the given solutions were carefully adjusted to pH 2-10 (pH meter model: BOECO BT-600, Germany) by adding either 0.01N HCl or NaOH solution. After equilibration for 24 h with continuous shaking the final pH ( $pH_f$ ) values of all these suspensions were recorded and the difference among the initial and final pH values [ $\Delta pH = pH_f - pH_i$ ] was plotted against the  $pH_i$ . The point that intersection the obtained curve at  $\Delta pH = 0$ , gave the value of point of zero charge (PZC).

## 2.6 Adsorption equilibrium experiments

The batch method was used for equilibrium study because of its simplicity. Solutions of MB having initial concentration  $10 \text{ mg.L}^{-1}$  were treated with 20, 30, 40, 50, 60, 80, 100 and 150  $\text{mg.L}^{-1}$  of PVA- $MF_{mag}$  nanoparticles respectively. The mixture was allowed to agitate for 1 h in dark chamber to attain adsorption-desorption equilibrium at controlled temperature. To observe the effect of temperature, a fixed amount of adsorbent ( $50 \text{ mg.L}^{-1}$ ) were agitated with various concentrations of dye ( $5\text{--}20 \text{ mg.L}^{-1}$ ) at three different temperatures (303, 313 and 323 K). After 1 h, the dye-loaded nanoparticles were separated by placing permanent magnet across the flask wall and the residual MB concentration in supernatant liquid was determined using UV-visible spectrophotometer (Spectronic 601) at wavelength 665 nm. The amount of MB uptake (Q) by PVA- $MF_{mag}$  nanoparticles and the percent removal (%R) of dye for each experiment were calculated by using equations 1 and 2, respectively.

$$Q = ((C_o - C)/m) \cdot V \quad (1)$$

$$\%R = ((C_o - C)/C_o) \cdot 100 \quad (2)$$

Where; Q is the amount of dye adsorbed by PVA- $MF_{mag}$  ( $\text{mg.g}^{-1}$ ), V is the volume of solution (L), m is the adsorbent weight (g), and  $C_o$  and C are the initial and final concentrations of dye ( $\text{mg.L}^{-1}$ ), respectively.

## 2.7 Adsorption kinetic experiments

For adsorption kinetic studies, 5, 10, 15 and 20  $\text{mg.L}^{-1}$  of methylene blue (MB) solutions were treated with 50  $\text{mg.L}^{-1}$  of PVA- $MF_{mag}$  nanoparticles at constant temperature of 303 K. The mixtures were incubated in dark chamber with continuous shaking. In all cases, pH was not adjusted and working pH was that of the solution. At appropriate intervals of time (5, 10, 20, 30, 45, 60 and 100 min), samples were taken and analyzed for residual MB concentration using UV-Vis spectrophotometer.

## 2.8 Effect of pH experiments

To investigate the effect of pH on adsorption of MB, a series of flasks, each containing 50  $\text{mg.L}^{-1}$  of PVA- $MF_{mag}$  dispersed in 10  $\text{mg.L}^{-1}$  MB solution, was assembled. The initial pH of the solutions were adjusted from 2–10 using 0.01 M HCl and NaOH. After shaking for 1 h, the dye-loaded nanoparticles were separated by placing permanent magnet across the container. In each experiment, the liquid portion was analysed for residual MB concentration by UV-visible spectrophotometer.

# 3. Results and Discussion

## 3.1 Characterization of adsorbent

### 3.1.1 Morphological and Elemental Analysis

Homogeneously dispersed uniform spherical  $MF_{mag}$  particles were successfully synthesized by the surfactant-free chemical coprecipitation method. As such, the applied precipitation conditions were systematically optimized with respect to concentration, reaction temperature and aging time to establish recipe for the production of uniform fine particles of Mn-Fe oxide. Uniformity in particle size and morphology is necessary to obtain batch-to-batch reproducible results in actual applications. Figure 2(a) depicts the scanning electron micrograph (SEM)

of the MF<sub>mag</sub> nanoparticles. The elemental composition of the same particles was determined by energy dispersive x-ray (EDX) analysis and the obtained spectra is shown in Figure 2(b). The EDX results showed the presence of Mn, Fe and O as the main components of the synthesized particles, however, traces of C, Si and Ca were also detected which might have leached out from the glassware and/or came from the precursor chemicals.

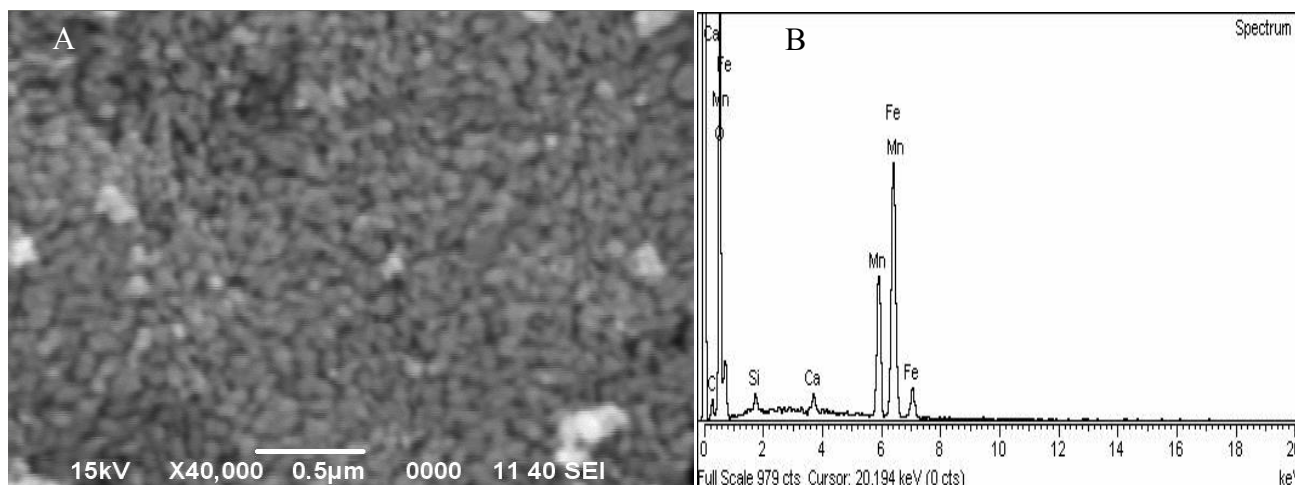


**Figure 2.** (A) Scanning electron micrograph (SEM) of MF<sub>mag</sub> nanoparticles and (B) the Energy dispersive x-ray (EDX) spectrum of the same particles.

### 3.1.2 Structural Analysis

X-rays diffraction analysis was performed on MF<sub>mag</sub> particles and the recorded pattern is depicted in Figure 3. As can be seen, the peaks observed at  $2\theta = 24.22^\circ$ ,  $33.33^\circ$ ,  $35.64^\circ$ ,  $40.94^\circ$ ,  $49.50^\circ$ ,  $54.14^\circ$ ,  $62.52^\circ$  and  $64.04^\circ$  were reflections from (012), (104), (110), (113), (024), (116), (214) and (300) planes of the rhombohedral crystal of hematite belonging to the space group  $R\bar{3}c$ . Kandori et al. have also reported the maximum intensity of hematite at  $2\theta = 33.3^\circ$  [25]. Similarly, peaks at  $2\theta = 29.7^\circ$ ,  $34.95^\circ$ ,  $36.61^\circ$ ,  $42.4^\circ$ ,  $55.96^\circ$ ,  $61.6^\circ$  and  $72.8^\circ$  were identified as the reflections from (220), (311), (222), (400), (511), (440) and (533) planes of cubic spinel crystals of manganese ferrite (Jacobsite, syn) having space group  $Fd\bar{3}m$  [26].

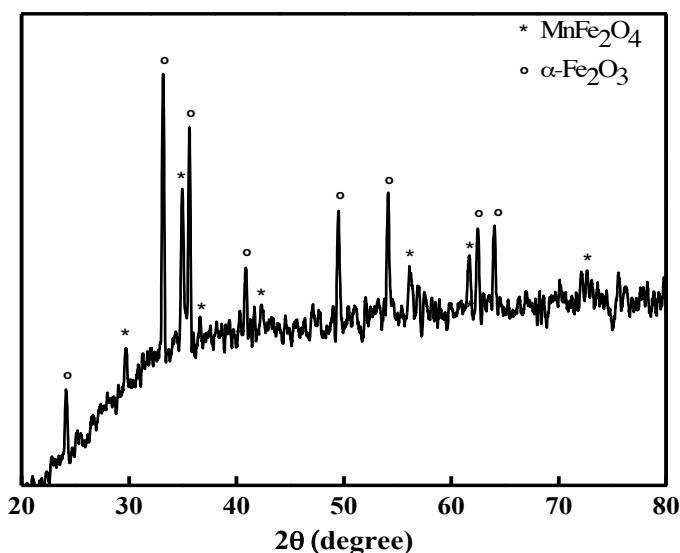


**Figure 3.** X-ray diffractogram (XRD) of the MF<sub>mag</sub> particles, shown in Fig. 2A.

The NIST software CMPR/LOGIC that contained a database of the card numbers from Powder Diffraction Files (PDF) assigned card numbers(1-1053D) and (10-319) to the hematite and manganese ferrite phases, respectively. Scherrer equation (Eq. 3) [27] was used to estimate the crystallite size of the heat treated crystalline materials from the major diffracted peak located at  $2\theta = 33.33^\circ$  for hematite phase and  $34.95^\circ$  for manganese ferrite.

$$D_p = (0.94\lambda) / (\beta \cos\theta) \quad (3)$$

Where

$D_p$  = crystallite size

$\lambda = 1.54 \text{ \AA}$

$\beta$  = the line broadening at half maximum intensity (FWHM)

$\theta$  = Bragg's angle

The crystallite size was found to be 58nm for hematite phase and 60 nm for ferrite phase in the present sample. The deviation of XRD curve from zero value of ordinate might be an indication of presence of some amorphous phase in the sample. Though the sample is biphasic, however, it shows magnetism and hence the material seems novel for application as magnetic support to the adsorbent for removal of organic dyes.

### 3.1.3 Point of zero charge

Following the procedure mentioned in section 2.5, the point of zero charge of the PVA-functionalized particles was found to be 4.8, as shown in Figure 4.

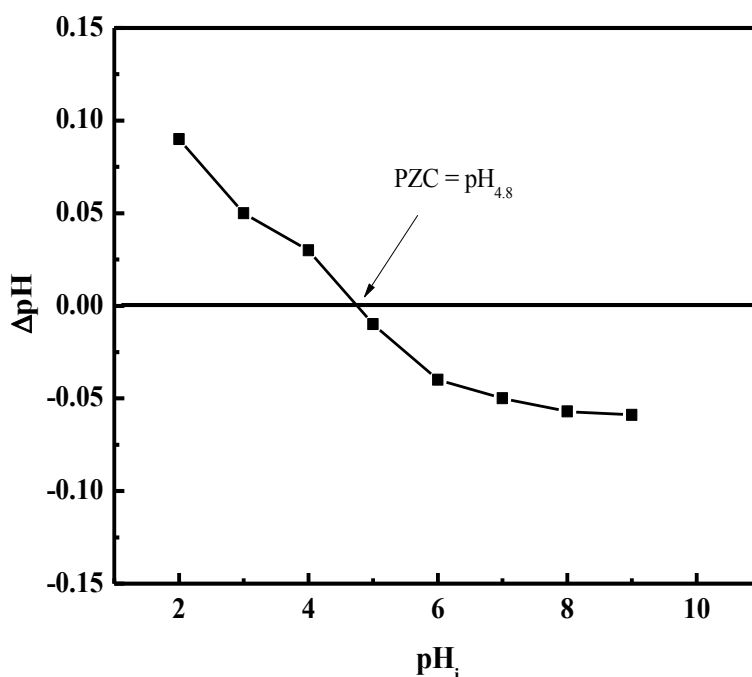


**Figure 4.** The Point of Zero Charge plot of PVA-MF<sub>mag</sub> nanoparticles

## 3.2 Adsorption Study

### 3.2.1 Effect of adsorbent dosage

Optimization of adsorbent dosage is important in order to determine the adsorption capacity for a given initial concentration ( $10 \text{ mg.L}^{-1}$  in current study) of dye solution. Figure 5 demonstrate the effect of adsorbent dose on the percentage removal of MB dye by PVA-MF<sub>mag</sub> nanoparticles. It is observed that dye adsorption increased with the increase in adsorbent dosage from 20-150  $\text{mg.L}^{-1}$ , however maximum adsorption of dye was observed in case of 50  $\text{mg.L}^{-1}$  dose of adsorbent. A slight decrease in adsorption capacity of adsorbent above 50  $\text{mg.L}^{-1}$  might be due to the increase in exchangeable site for a given amount of dye molecules.

### 3.2.2 Effect of pH

pH of the dye solution is one of the leading factors to monitor adsorption process by controlling the magnitude of electrostatic charges imparted by ionized dye molecules and adsorbent surface [28]. As is clear from Figure 6, a regular increase in adsorption capacity of the PVA-MF<sub>mag</sub> nanoparticles was observed with the increase in pH from 2–6 and then became almost invariable. This phenomenon can be explained by taking into account the PZC of adsorbent (PZC = 4.8). At  $pH > pH_{pzc}$ , the PVA surface acquires negative charge due to deprotonation and below PZC the surface of adsorbent is positively charged. Therefore, the increase in adsorption capacity with pH is attributed to the deprotonation of PVA, which provide negatively charged adsorbent sites, thereby favoring the adsorption of positively charged dye cations because of the electrostatic attraction. Furthermore,

poorer adsorption of MB at pH below 6 is possibly due to the existence of surplus  $H^+$  ions which compete with the positively charged dye for adsorption onto the available adsorption sites [6, 23]. Umorin et al. [23] found maximum adsorption of MB onto PVA gel at pH = 4 which was below PZC (4.3) of the adsorbent they determined. In the present case, maximum adsorption occurred around pH 6, which is in line with many studies conducted on adsorption of MB onto various adsorbents [1, 29].

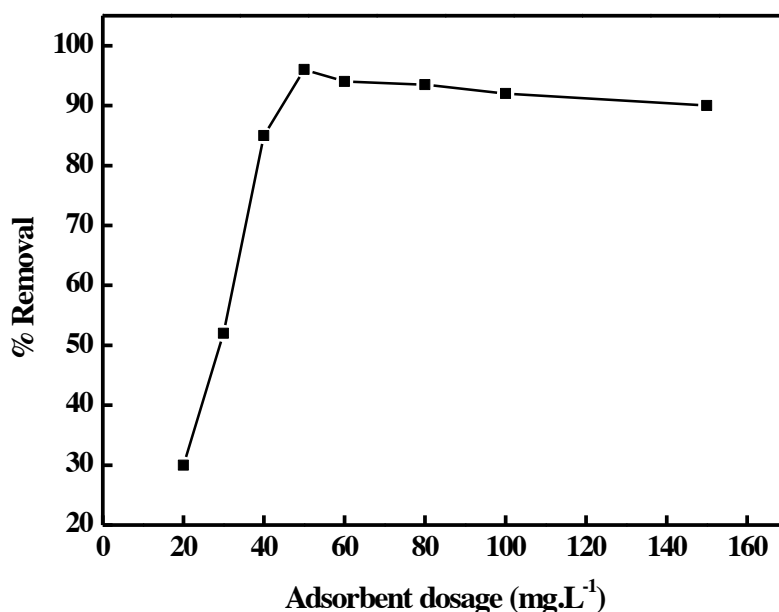


**Figure 5.** Effect of adsorbent dosage on the adsorption capacity of PVA-MF<sub>mag</sub> nanoparticles.

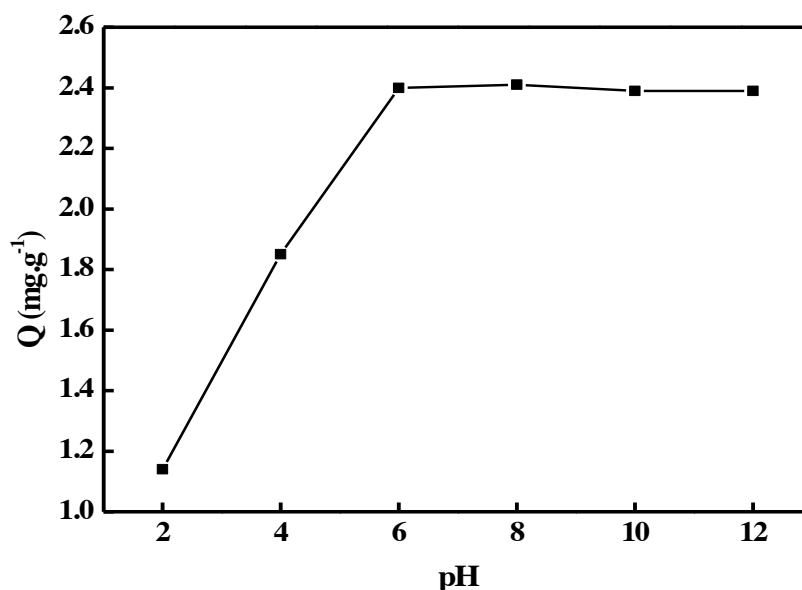


**Figure 6.** Effect of initial pH of dye solution on the adsorption of MB onto PVA-MF<sub>mag</sub> nanoparticles. Experimental conditions:  $m = 50 \text{ mg.L}^{-1}$ ,  $T = 303 \text{ K}$ , MB conc. =  $10 \text{ mg.L}^{-1}$ , pH = 6.

### 3.2.3 Effect of initial concentration of MB and contact time

The initial dye concentration factor describes an immediate relation between the dye concentration and the available binding sites on an adsorbent surface. In general, the percent removal of dye is inversely related to its initial concentration. At lower concentration, there will be vacant adsorption sites on the surface of adsorbent, which become fewer for higher initial dye concentration. However, the increase in the initial dye concentration will cause an increase in the loading capacity of the adsorbent by the virtue of high driving force for mass at a high initial dye concentration [23].

The effect of initial dye concentration and contact time on the adsorption of MB onto PVA-MF<sub>mag</sub> is given in Figure 7. As can be seen from this figure, when the initial MB concentration is increased from 5 to 20 mg.L<sup>-1</sup>, the amount of MB adsorbed per unit weight of the PVA-MF<sub>mag</sub>(mg.g<sup>-1</sup>) increased from 2.5 to 6. Consequently, the percent removal decreased from 99% to 59% (see Figure 8) while the extent of adsorption increased linearly with initial dye concentration. Similar trend was reported elsewhere [21, 22] for the adsorption of species of interest from aqueous solutions. It is an understandable fact that the initial concentration of MB offers a vital driving force to overwhelm all of the mass transfer resistance. For the same amount of adsorbent, the available adsorption sites became less for higher initial concentration of dye and hence the removal of MB is dependent on the initial concentration. The adsorption of MB onto PVA-MF<sub>mag</sub> was observed to be fast enough at the initial period of contact time, and then slowed down with the passage of time, obviously due to saturation of the adsorbent surface with the adsorbate molecules.

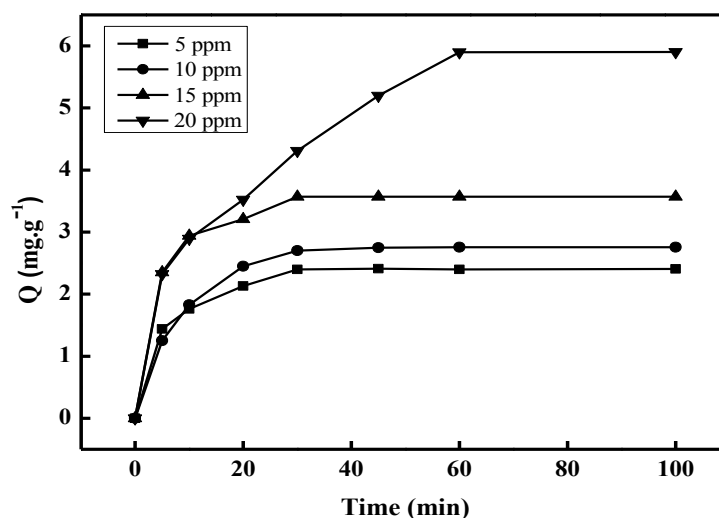


**Figure 7.** Effect of contact time on the adsorption of MB onto PVA- MF<sub>mag</sub> nanoparticles. Experimental conditions:  $m = 50 \text{ mg.L}^{-1}$ ,  $T = 303 \text{ K}$ ,  $C = 5\text{--}20 \text{ mg.L}^{-1}$ ,  $\text{pH} = 6$ .

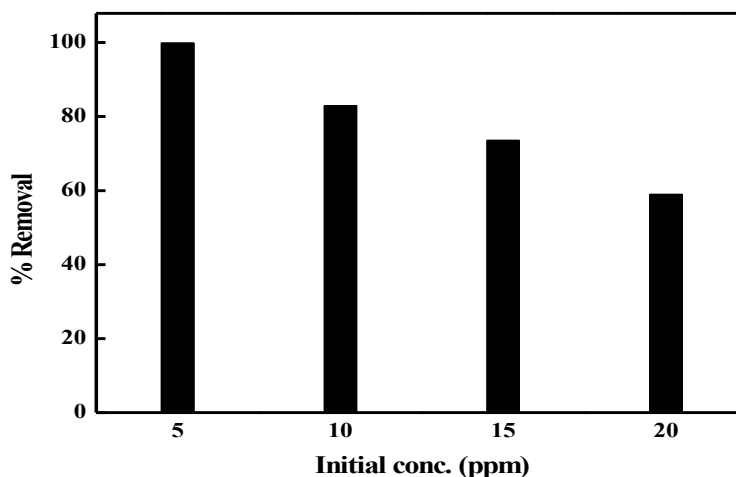


**Figure 8.** Effect of initial dye concentration on the adsorption percentage of MB onto PVA-MF<sub>mag</sub> nanoparticles

### 3.3 Adsorption kinetics

In order to interpret the adsorption mechanism, Lagergren Pseudo-first order and pseudo-second order kinetic models were applied to experimental data. Eq. 4 represents the Lagergren pseudo-first order kinetic model [30].

$$\ln(q_e - q_t) = \ln q_e - k_1 t \quad (4)$$

where,  $q_e$  and  $q_t$  denote the quantity of dye adsorbed (mg.g<sup>-1</sup>) at equilibrium and time  $t$  (min).  $k_1$  (min<sup>-1</sup>) is pseudo-first order rate constant. The values of rate constant and equilibrium adsorption density can be calculated from slope and intercept of plot  $\ln(q_e - q_t)$  vs  $t$  for various dye concentration at temperature 303 K (Figure 9). It is clear from the plot that experimental data of current study do not follow the Lagergren pseudo-first order

kinetics for all dye concentrations and entire adsorption course. The calculated adsorption capacity  $q_e$  ( $\text{mg}\cdot\text{g}^{-1}$ ) does not match with the experimental data. The non-fitting of pseudo-first order model to MB adsorption onto adsorbent has been published [23].

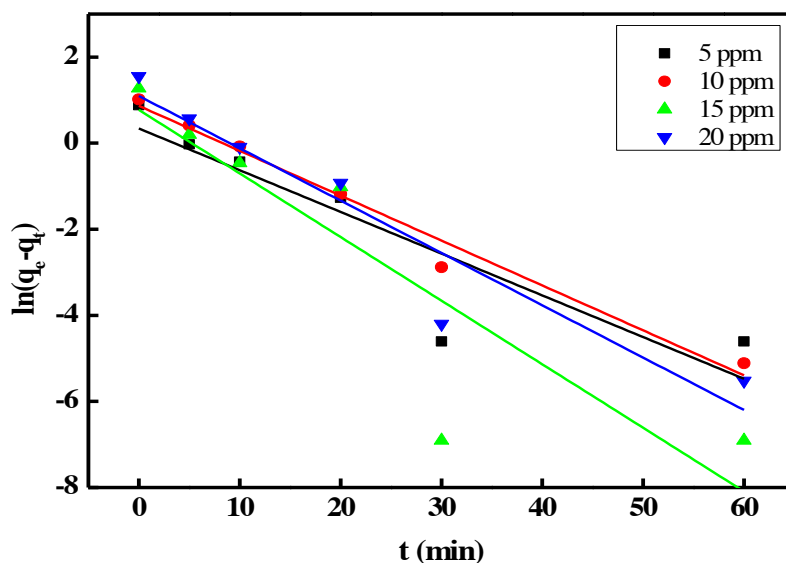


**Figure 9.** Pseudo-first order kinetic plot for the adsorption of MB onto PVA-MF<sub>mag</sub> nanoparticles.

The pseudo-second order kinetic model is represented in Eq. 5 [30], given below.

$$t/q_t = 1/(k_2 \cdot q_e^2) + t/q_e \quad (5)$$

where  $k_2$  ( $\text{g}\cdot\text{mg}^{-1}\cdot\text{min}^{-1}$ ) is the rate constant. The values of  $q_e$  and  $k_2$  can be calculated from slope and intercept of the linear plot of  $t/q_t$  vs  $t$ , respectively (Figure 10).

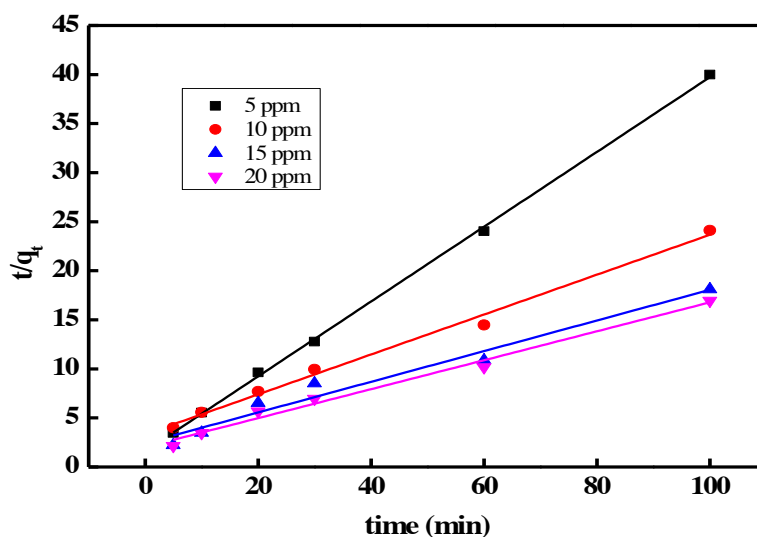


**Figure 10.** Pseudo-second order kinetic plot for the adsorption of MB onto PVA-MF<sub>mag</sub> nanoparticles.

Among the applied kinetic models, pseudo-second order is the best fit to interpret the mechanism of adsorption. The linear plots of  $t/q_t$  vs  $t$  for various initial concentrations of dye showed good agreement between the experimental and calculated  $q_e$  values. Moreover, the values of correlation coefficients of pseudo-second order ( $R^2 = 0.99$ ) were greater than that of pseudo-first-order kinetic model. Consequently, it can be concluded that adsorption data fit well into pseudo-second-order model. These results are in accordance with previous studies on adsorption of MB onto various adsorbents [31, 32]. The kinetic data obtained from the above-mentioned kinetic models has been summarized in table 1.

**Table 1.** Adsorption kinetic parameters calculated for adsorption of MB onto PVA-MFmag nanoparticles at 303 K

Conc. of dye(mg.L <sup>-1</sup> )	q <sub>e</sub> exp. (mg.g <sup>-1</sup> )	Pseudo-first order			Pseudo-second order		
		K <sub>1</sub> (min <sup>-1</sup> )	q <sub>e</sub> cal. (mg.g <sup>-1</sup> )	R <sup>2</sup>	K <sub>2</sub> (g.mg <sup>-1</sup> .min <sup>-1</sup> )	q <sub>e</sub> cal. (mg.g <sup>-1</sup> )	R <sup>2</sup>
5	2.5	0.09695	1.40818	0.761	0.0903	2.62	0.99929
10	4.38	0.10434	2.3813	0.976	0.0124	4.917	0.99155
15	5.52	0.14777	2.17	0.743	0.0100	6.40	0.96253
20	6.0	0.1216	2.9979	0.8869	0.0107	6.78	0.98575

### 3.4 Adsorption isotherms

Adsorption isotherm is an important model to describe the adsorption behavior of solid-liquid adsorption system. At equilibrium state, the adsorption isotherm emphasize the distribution of adsorbate molecules between the two phases of the system. In order to understand the adsorption behavior, it is significant to identify the suitable adsorption isotherm model. In the present investigation, Freundlich, Langmuir and Temkin adsorption isotherm models were applied to the experimental data obtained at 303, 313 and 323 K.

According to Langmuir isotherm theory, adsorption takes place on specific homogeneous sites of adsorbent surface. This isotherm has found successful application in many sorption processes. The linear form of Langmuir's isotherm model is represented by the following equation [30]:

$$C_e/q_e = 1/q_0K_L + C_e/q_0 \quad (6)$$

Where q<sub>0</sub> (mg g<sup>-1</sup>) gives the monolayer adsorption capacity and the constant K<sub>L</sub>(L.mg<sup>-1</sup>) is related to energy of adsorption. The values of q<sub>0</sub> and K<sub>L</sub> can be calculated from the slope and intercept of the linear plot C<sub>e</sub>/q<sub>e</sub> versus C<sub>e</sub>(Figure 11).

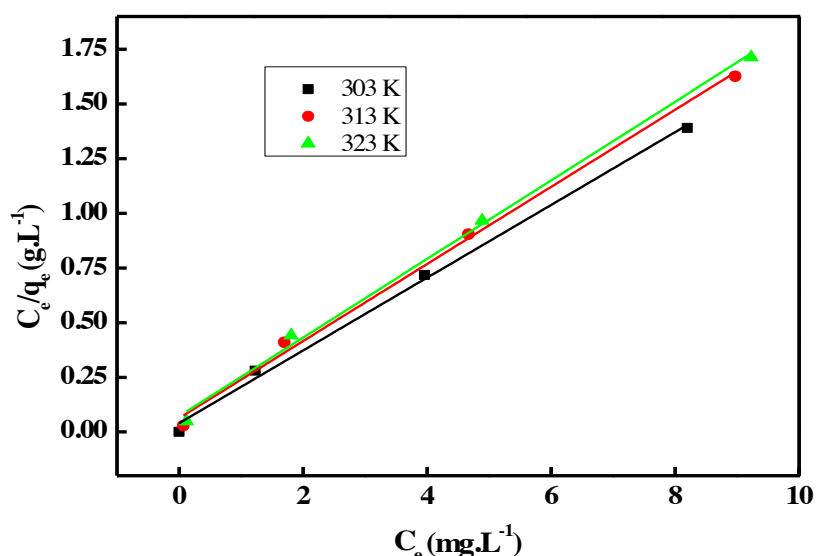


**Figure 11.** Langmuir's isotherm plot for the adsorption of MB onto PVA-MF<sub>mag</sub> nanoparticles.

The favorable nature of adsorption can be expressed in terms of dimensionless separation factor of equilibrium parameter (R<sub>L</sub>), which is defined by eqn 7 [30]:

$$R_L = 1/(1 + K_L C_0) \quad (7)$$

The value of R<sub>L</sub> indicates the type of isotherm to be either irreversible (R<sub>L</sub> = 0), linear (R<sub>L</sub> = 1), unfavorable (R<sub>L</sub> > 1) or favorable (1 < R<sub>L</sub> < 0) [6]. In the current study, the values of R<sub>L</sub> for methylene blue adsorption onto PVA-MF<sub>mag</sub> nanoparticles at different temperature were found between zero and 1 which clearly indicate favorable adsorption. The linear decrease in the value of K<sub>L</sub> with increase in temperature is the indication of decrease of adsorption energy at higher temperatures.

The surface area of the adsorbent particles can be estimated from Langmuir's isotherm using the following equation [33]:

$$S. A = (q_{\max} \cdot N \cdot A) / M \quad (8)$$

Where  $q_{\max}$  is the monolayer capacity,  $N$  is avogadro's number,  $A$  is the area of one molecule of MB ( $120 \text{ \AA}^2$ ) and  $M$  is the molecular mass of MB ( $373.9 \text{ g}$ ). The surface area of PVA-MF<sub>mag</sub> nanoparticles comes out to  $12.58 \text{ m}^2 \cdot \text{g}^{-1}$ .

The Freundlich isotherm is an empirical equation describing adsorption equilibrium on heterogeneous surfaces and hence does not assume monolayer capacity. The linear form of Freundlich equation is given below [30]:

$$\ln q_e = \ln K_F + (1/n) \ln C_e \quad (9)$$

where the constants  $K_F (\text{mg} \cdot \text{g}^{-1} (\text{L} \cdot \text{mg}^{-1})^{1/n})$  and  $n$  represent adsorption capacity and adsorption strength, respectively. The values of  $K_F$  and  $n$  were calculated from the slope and intercept of the linear plot  $\ln q_e$  versus  $\ln C_e$  (Figure 12). The slope ( $1/n$ ) having value ( $1 > 1/n > 0$ ) is a measure of adsorption intensity or surface heterogeneity. It becomes more heterogeneous as its value gets closer to zero. The value of  $1/n$  below one indicates a normal Langmuir isotherm while  $1/n$  above one is indicative of cooperative adsorption mechanism.

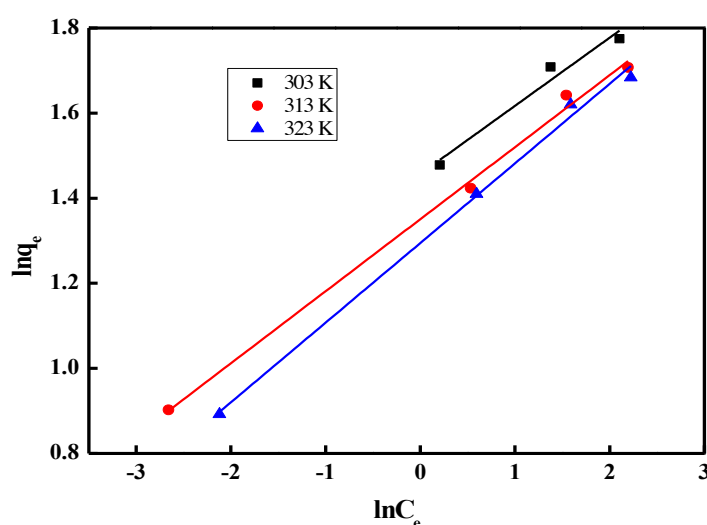


**Figure 12.** Freundlich isotherm plot for the adsorption of MB onto PVA-MF<sub>mag</sub> nanoparticles.

Table 2 shows that values of  $1/n$  for adsorption of MB onto PVA-MF<sub>mag</sub> nanoparticles at different temperatures are ranging between zero and one. The decrease in the value of  $K_F$  with higher temperatures pointed towards the decrease in adoption capacity, i.e., the lower the temperature the greater the adsorption of MB onto PVA-MF<sub>mag</sub> nanoparticles.

**Table 2.** Isotherm parameter for the adsorption of MB on PVA-MF<sub>mag</sub> nanoparticles

Model	Parameter	Temperature (K)		
		303	313	323
Langmuir isotherm	$q_{\max} (\text{mg} \cdot \text{g}^{-1})$	6.01106	5.67247	5.56359
	$K_L$	4.152398	2.796923	2.499165
	$R_L$	0.1189	0.0176	0.0196
	$R^2$	0.99531	0.9947	0.9956
Freundlich isotherm	$K_F (\text{mg}^{1-1/n} \cdot \text{L}^{1/n} \cdot \text{g}^{-1})$	4.29263	3.85997	3.64957
	$1/n$	0.1602	0.1693	0.1872
	$R^2$	0.93961	0.99461	0.9938
Temkin isotherm	$B_T$	0.44529	0.63043	0.68708
	$K_T$	43466.10	637.03	272.00
	$R^2$	0.93757	0.97622	0.9880

Temkin isotherm model take into account the effect of indirect adsorbent-adsorbate interactions on adsorption, and suggests that the heat of adsorption of all the molecules in the layer would decrease linearly with coverage

due to these interactions [23]. This model further assumes that adsorption is characterized by a uniform distribution of binding energies, up to some maximum binding energy. The Temkin isotherm is commonly applied in the following form [23]:

$$q_e = B_T \ln K_T + B_T \ln C_e \quad (10)$$

where  $K_T$  is the equilibrium binding constant ( $L \cdot mg^{-1}$ ) and  $B_T$  is the Temkin constant related to the heat of adsorption. The constant  $K_T$  and  $B_T$  were calculated from the plot of  $q_e$  versus  $\ln C_e$  (Figure 13) and summarized in Table 2. The Temkin constant,  $B_T$ , showed that the heat of adsorption of MB onto PVA-MF<sub>mag</sub> nanoparticles showed a linear increase in value at higher temperatures indicating an exothermic process.

By comparing the isotherm models for the adsorption of MB onto PVA-MF<sub>mag</sub> nanoparticles, it could be inferred that all the three isotherm models closely fitted the experimental data as revealed with good regression coefficients ( $R^2 > 0.9$ ) in the concentration range studied (Table 2). However, the regression results showed that the Langmuir's model fitted the experimental data better than the others did.

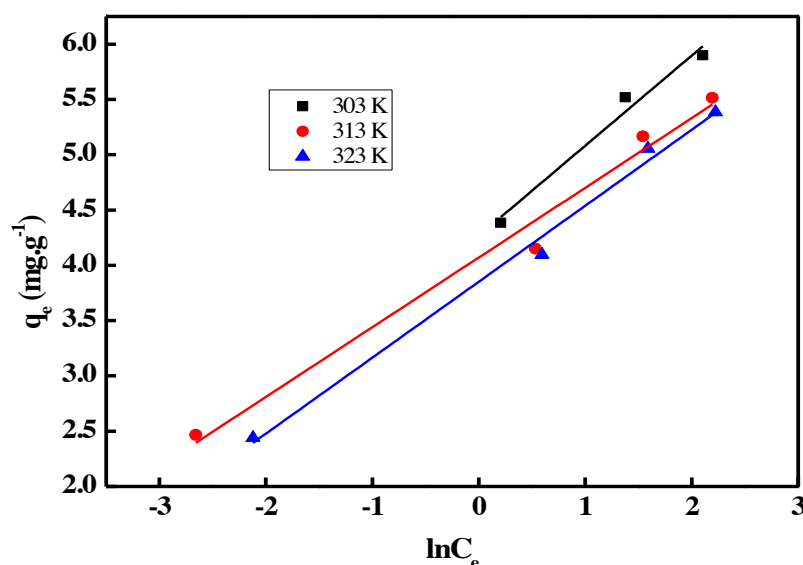


**Figure 13.** Temkin isotherm plot for the adsorption of MB onto PVA-MF<sub>mag</sub> nanoparticles.

### 3.5 Adsorption Thermodynamics

In order to study the thermodynamics of adsorption of MB on PVA-MF<sub>mag</sub> nanoparticles, three basic thermodynamic parameters, enthalpy ( $\Delta H^\circ$ ), entropy ( $\Delta S^\circ$ ) and Gibbs free energy ( $\Delta G^\circ$ ), were calculated using following equations [30]:

$$K_D = q_e/C_e \quad (11)$$

$$\Delta G = -RT \ln K_D \quad (12)$$

$$\ln K_D = \Delta S^\circ/R - \Delta H^\circ/RT \quad (13)$$

Where,  $T$  is the solution temperature (K),  $K_D$  is the adsorption equilibrium constant, and  $R$  is the gas constant ( $8.314 J \cdot mol^{-1}$ ). The values of enthalpy ( $\Delta H^\circ$ ) and entropy ( $\Delta S^\circ$ ) were calculated from the slope and intercept of the linear plot of  $\ln q_e/C_e$  vs  $1/T$ , as shown in Figure 14. Gibbs free energy was calculated using eq. 12. The values of thermodynamic parameters are listed in Table 3.

The negative value of  $\Delta H^\circ$  indicated the exothermic nature of the adsorption of MB onto PVA-MF<sub>mag</sub> nanoparticles. Kara et al. [34] suggested that the  $\Delta H^\circ$  of physisorption is smaller than  $40 kJ \cdot mol^{-1}$ . In the present investigation,  $\Delta H^\circ$  was calculated to be  $-33.095 kJ \cdot mol^{-1}$ , which confirmed the physical adsorption of MB onto synthesized adsorbent.

The criterion for spontaneity of a reaction is change in Gibb's free energy. For physical adsorption,  $\Delta G$  value is between  $-20$  and  $0 kJ \cdot mol^{-1}$ , for physio-chemisorption its values range between  $-80$  and  $-20 kJ \cdot mol^{-1}$ , and for chemisorption it is at  $-80$  and  $-400 kJ \cdot mol^{-1}$  [30]. The Gibbs free energy values are negative in the temperature range  $303$ – $323$  K, inferring that the adsorption process is spontaneous and thermodynamically favorable. With the increase in temperature from  $303$  to  $323$  K, the value of  $\Delta G^\circ$  increased from  $-4.2$  to  $-1.4 kJ \cdot mol^{-1}$ , suggested

that lower temperature favored maximum adsorption. The negative value of change in entropy ( $\Delta S^\circ$ ) depicted the decrease in the degree of freedom of adsorption of MB onto PVA-MF<sub>mag</sub> nanoparticles. Before adsorption, the molecules of MB dye were free to move in any direction but once they adsorbed to the surface of PVA-MF<sub>mag</sub> nanoparticles, their motion was restricted leading to an ordered arrangement and hence entropy decreased.

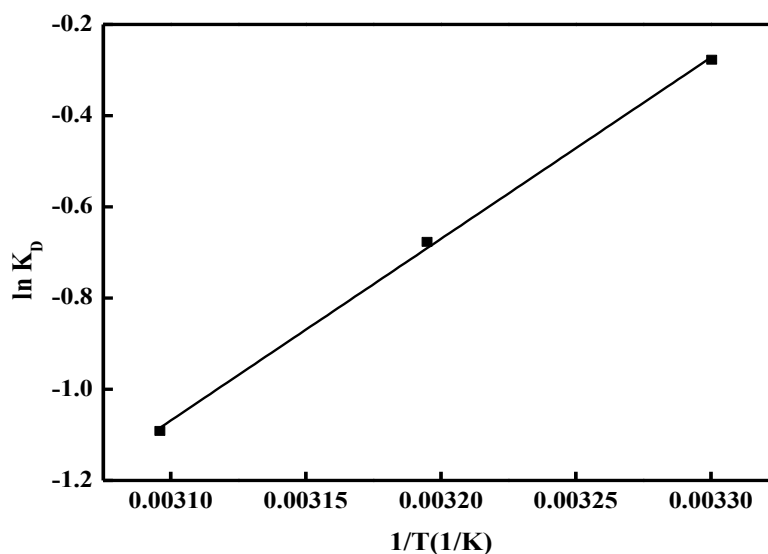


**Figure 14.** Plot of  $\ln K$  versus  $1/T$  for the estimation of thermodynamic parameters.

**Table 3.** Thermodynamic parameters for the uptake of MB (adsorbent dose (m) = 50mg.L<sup>-1</sup>)

- $\Delta G$ (kJ.mol <sup>-1</sup> )			- $\Delta S$ (j.mol <sup>-1</sup> .K)	- $\Delta H$ (kJ.mol <sup>-1</sup> )
303 K	313 K	323 K		
4.216	2.215	1.410	111.47	33.095

### 3.6 Recovery of Adsorbent (PVA-MF<sub>mag</sub>)

The adsorbent was successfully collected by applying a permanent magnet along the wall of the adsorption vessel, as shown in Figure 15. Preliminary experiments revealed that the adsorbed dye could be successfully removed from the magnetically collected adsorbent by heat treatment at 473 K for a period of 1 h. In fact, the surface PVA started degradation into CO<sub>2</sub> at the mentioned temperature [24], which in turn took away the adsorbed dye and leaving behind the bare surface of MF<sub>mag</sub> nanoparticles. Work is going in our laboratory for assessing the recycling of this material for further use.

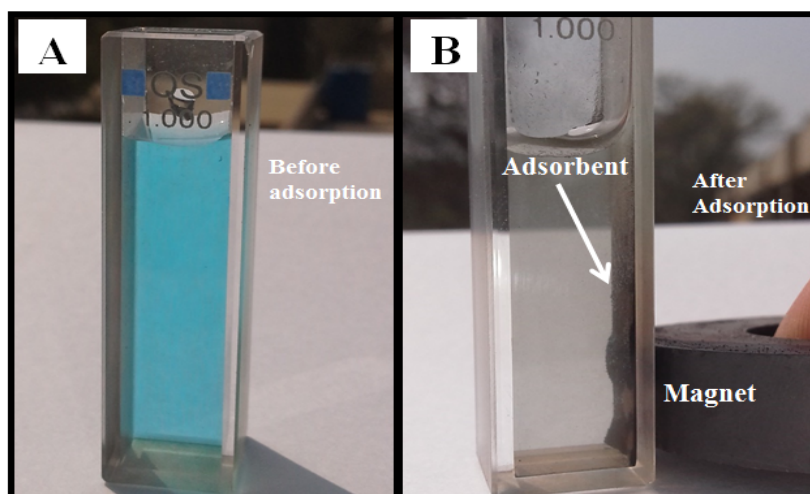


**Figure 15.** Photographs of MB solution (A) before adsorption and (B) after adsorption onto PVA-MF<sub>mag</sub> nanoparticles at pH = 6.

## Conclusions

- Ultra-fine Mn-Fe oxide nanoparticles with uniform spherical morphology were successfully synthesized via controlled chemical coprecipitation route.
- On controlled heat treatment at 1173 K, the as-prepared particles of Mn-Fe oxide transformed into magnetic particles without sintering.
- The magnetic Mn-Fe oxide particles were successfully functionalized with nontoxic and low priced polymer -polyvinyl alcohol (PVA).
- The functionalized magnetic particles possessed the efficiency of fast removal of methylene blue dye from aqueous solutions. Up to 99% removal of dye was achieved within 1 h at 303 K under optimized experimental conditions.
- Experimental data best fitted into pseudo-second order equation.
- Freundlich, Langmuir and Temkin adsorption isotherms are applicable, however, Langmuir model was found best fit to the experimental data.
- The amount of dye adsorbed on PVA-MF<sub>mag</sub> particles linearly decreased with the increase in temperature.
- $\Delta G^\circ$  and  $\Delta H^\circ$  values suggested that the adsorption process is spontaneous, exothermic and physical in nature.

**Acknowledgments-** The authors are pleased to acknowledge National Centre of Excellence in Physical Chemistry, University of Peshawar, Peshawar-25120, Khyber Pakhtunkhwa, Pakistan for facilitating this research work.

## References

1. T. Ainane, F. Khammour, M. Talbi, *Oriental J. Chem.* 30 (2014) 1183-1189.
2. VK. Garg, M. Amita, R. Kumar, R. Gupta, *Dyes Pigm.* 63 (2004) 243-250.
3. L. Wang, J. Zhang, A. Wang, *Colloids Surf. A* 322 (2008) 47-53.
4. H. Lata, VK. Garg, RK. Gupta, *Dyes Pigm.* 74 (2007) 653-658.
5. XS. Wang, Y. Zhou, Y. Jiang, C. Sun, *J. Hazard. Mater.* 157 (2008) 374-385.
6. Z. Shahryari, AS. Goharrizi, M. Azadi, *Int. J Water Res Environ Eng.* 2 (2010) 16-28.
7. M. Panizza, A. Barbucci, R. Ricotti, G. Cerisola, *Sep. Purif. Technol.* 54 (2007) 382-387.
8. TH. Kim, C. Park, J. Yang, S. Kim, *J. Hazard. Mater.* 112 (2004) 95-103.
9. K. Dutta, S. Mukhopadhyay, S. Bhattacharjee, B. Chaudhuri, *J. Hazard. Mater.* 84 (2001) 57-71.
10. G. Muthuraman, TT. Teng, CP. Leh, I. Norli, *J. Hazard. Mater.* 163 (2009) 363-369.
11. M. Rafatulla., O. Sulaiman, R. Hashim, A. Ahmad, *J. Hazard. Mater.* 177 (2010) 70-80.
12. B. Hameed, AM. Din, A. Ahmad, *J. Hazard. Mater.* 141 (2007) 819-825.
13. B. Hameed, A. Ahmad, K. Latiff, *Dyes Pigm.* 75 (2007) 143-149.
14. S. Chakrabarti, BK. Dutta, *J. Colloid Interface Sci.* 286 (2005) 807-811.
15. Vadivelan V., Kumar K.V., *J. Colloid Interface Sci.* 286 (2005) 90-100.
16. D. Özer, G. Dursun, A. Özer, *J. Hazard. Mater.* 144 (2007) 171-179.
17. CH. Weng, YT. Lin, TW. Tzeng, *J. Hazard. Mater.* 179 (2009) 417-424.
18. N. Barka, A. Assabbane, A. Nounah, L. Laanab, YA. Ichou, *Desalination* 235 (2009) 264-275.
19. KV. Kumar, V. Ramamurthi, S. Sivanesan, *J. Colloid Interface Sci.* 284 (2005) 14-21.
20. Z. Al-Qodah, W. Lafı, Z. Al-Anber., M. Al-Shannag, A. Harahsheh, *Desalination* 217 (2007) 212-224.
21. SB. Bukallah, M. Rauf, S. Ali, *Dyes Pigm.* 74 (2007) 85-87.
22. G. Crini, *Dyes Pigm.* 77 (2008) 415-426
23. S. Umoren, U. Etim, A. Israel, *J. Mater. Environ. Sci.* 4 (2013) 75-86.
24. S. Kayal, R. Ramanujan, *Mater. Sci. Eng. C* 30 (2010) 484-490.
25. K. Kandori, N. Hori, T. Ishikawa, *Colloids Surf. A* 290 (2006) 280-287.
26. Y. Jamil, MR. Ahmad, A. Hafeez, ZU. Haq, *Pak. J. Agr. Sci.* 45(2008) 59-64.
27. IU. Haq, K. Akhtar, ZU. Khan, *High Temp. Mater. Proc.* 34 (2015) 325-332.
28. R. Jain, M. Shrivastava, *J. Hazard. Mater.* 158 (2008) 549-556.
29. J. Jeyanthi, M. Dhinakaran, *J. Exp. Sci.* 3 (2012) 21-26
30. W. Konicki, D. Sibera, E. Mijowsk., Z. Lendzion-Bieluń, U. Narkiewicz, *J. Colloid interface Sci* 398(2013) 152-160.
31. X. Hou, J. Feng, Y. Ren, Z. Fan, M. Zhang, *Colloids Surf. A* 363(2010) 135-140.
32. R. Gottipati, S. Mishra, *J. Braz. J. Chem. Eng.* 27 (2010) 357-367.
33. J. Potgieter, *J. Chem. Edu.* 68(1991) 349-350
34. M. Kara, H. Yuzer, E. Sabah, M. Celik, *Water Res.* 37(2003) 224-232.

(2018) ; <http://www.jmaterenvirosci.com>